BJP British Journal of Pharmacology

DOI:10.1111/j.1476-5381.2012.01994.x
www.brjpharmacol.org

RESEARCH PAPER

3-Nitropropionic acid induces autophagy by forming mitochondrial permeability transition pores rather than activatiing the mitochondrial fission pathway

Maria E Solesio[1], Sara Saez-Atienzar[2], Joaquin Jordan[2] and Maria F Galindo[1]

[1]*Unidad de Neuropsicofarmacología Traslacional, Complejo Hospitalario Universitario de Albacete, Albacete, Spain, and* [2]*Grupo de Neurofarmacología, Dpto. Ciencias Médicas, Fac. de Medicina de Albacete, Universidad Castilla-La Mancha, IDINE, Albacete, Spain*

Correspondence
María F Galindo, Unidad de Neurofarmacología Traslacional, Complejo Hospitalario Universitario de Albacete, C/ Hermanos Falcó 37, 02006 Albacete. Spain. E-mail: mgalindoa@sescam.jccm.es

Keywords
Huntington's disease; mitochondrial dynamics; MPTP; Drp1; Bax; Mdivi-1; mitochondrial swelling

Received
5 December 2011
Revised
19 March 2012
Accepted
26 March 2012

BACKGROUND AND PURPOSE
Huntington's disease is a neurodegenerative process associated with mitochondrial alterations. Inhibitors of the electron–transport channel complex II, such as 3-nitropropionic acid (3NP), are used to study the molecular and cellular pathways involved in this disease. We studied the effect of 3NP on mitochondrial morphology and its involvement in macrophagy.

EXPERIMENTAL APPROACH
Pharmacological and biochemical methods were used to characterize the effects of 3NP on autophagy and mitochondrial morphology. SH-SY5Y cells were transfected with GFP-LC3, GFP-Drp1 or GFP-Bax to ascertain their role and intracellular localization after 3NP treatment using confocal microscopy.

KEY RESULTS
Untreated SH-SY5Y cells presented a long, tubular and filamentous net of mitochondria. After 3NP (5 mM) treatment, mitochondria became shorter and rounder. 3NP induced formation of mitochondrial permeability transition pores, both in cell cultures and in isolated liver mitochondria, and this process was inhibited by cyclosporin A. Participation of the mitochondrial fission pathway was excluded because 3NP did not induce translocation of the dynamin-related protein 1 (Drp1) to the mitochondria. The Drp1 inhibitor Mdivi-1 did not affect the observed changes in mitochondrial morphology. Finally, scavengers of reactive oxygen species failed to prevent mitochondrial alterations, while cyclosporin A, but not Mdivi-1, prevented the generation of ROS.

CONCLUSIONS AND IMPLICATIONS
There was a direct correlation between formation of mitochondrial permeability transition pores and autophagy induced by 3NP treatment. Activation of autophagy preceded the apoptotic process and was mediated, at least partly, by formation of reactive oxygen species and mitochondrial permeability transition pores.

LINKED ARTICLE
This article is commented on by González-Polo *et al.*, pp. 60–62 of this issue. To view this commentary visit http://dx.doi.org/10.1111/j.1476-5381.2012.02203.x

Abbreviations
3NP, 3-nitropropionic acid; CsA, cyclosporin A; DCFH-DA, 2′,7″-dichlorodihydrofluorescein diacetate; Drp1, Dynamin-related protein 1; Mdivi-1, mitochondrial division inhibitor-1; MnTBAP, Mn(III)tetrakis (4-benzoic acid)porphyrin

chloride; MOMP, mitochondrial outer membrane permeabilization; MPTP, mitochondrial permeability transition pore; ROS, reactive oxygen species; TEMPOL, 4-hydroxy-2,2,6,6-tetramethylpiperidine-N-oxyl; TMRM, tetramethylrhodamine methyl ester

Introduction

Macrophagy, here simply referred to as autophagy, is associated with cell death. The term autophagic (or type 2) cell death is also used frequently. In some circumstances, apoptosis and autophagy seem to be, positively or negatively interconnected, referring to the 'molecular switches' between them (Xue *et al.*, 1999; Yu *et al.*, 2006; Leber and Andrews, 2010). Undoubtedly, there are multiple connections between apoptotic and autophagic processes, which jointly can determine the fate of cells (Leber and Andrews, 2010). Autophagy plays a physiological role that is important for cellular homeostasis, and this requires a continuous turnover of non-functional proteins and organelles (Cuervo, 2004).

Mitochondria are considered multifunctional organelles of changing morphology. Cells continually adjust the rate of mitochondrial fission and fusion in response to changing energy demands and to facilitate the distribution of mitochondria (Detmer and Chan, 2007). These events are especially relevant within neurons where mitochondria need to be very active to meet the high energy demands. Mitochondrial malfunctioning has been observed in several neurodegenerative disorders, and inhibitors of mitochondrial respiration are frequently used to mimic neurodegenerative disorders (Browne and Beal, 2002). For instance, the succinate dehydrogenase inhibitor 3-nitropropionic acid (3NP) is commonly used to develop experimental models of Huntington's disease (Bove *et al.*, 2005) Extensive behavioural and neuropathological evaluations have shown that a partial but prolonged energy impairment induced by 3NP is sufficient to produce most of the clinical and pathophysiological hallmarks of Huntington's disease (Beal *et al.*, 1993; Brouillet *et al.*, 1999; Bove *et al.*, 2005). The molecular mechanisms involved in 3NP-induced neurotoxicity remains unclear. Nevertheless, participation of the intrinsic apoptosis pathway, which is critically dependent on mitochondrial outer membrane permeabilization (MOMP), and the consequent release of cell-death-mediating mitochondrial intermembrane space proteins, such as cytochrome c, has been described (Chipuk *et al.*, 2008). Before releasing apoptotic factors, mitochondria often display a dramatic morphological transformation, namely a thread-grain transition, which is mediated by mitochondrial fission proteins (Skulachev *et al.*, 2004; Gomez-Lazaro *et al.*, 2008a). Swollen mitochondria have been observed in the context of neurodegenerative diseases (Menzies *et al.*, 2002; Ferreirinha *et al.*, 2004), and this has been related to the involvement of the mitochondrial permeability transition pore (MPTP) (Crompton, 1999). Under *in vitro* , pseudopathological, conditions of oxidative stress, with relatively high levels of reactive oxygen species (ROS), Ca^{2+} and low ATP, the complex flickers into an open-pore state, allowing free diffusion of solutes across the inner membrane (Crompton, 1999). On the other hand, Bcl-2 family members, such as Bax, can form ion-selective channels and larger diameter pores, resulting in the release of pro-apoptotic proteins (Antignani and Youle, 2006). Recent studies have proposed that mitochondrial fission is an additional or alternative mechanism in the mitochondrial pathway of apoptosis (Frank *et al.*, 2001; Bossy-Wetzel *et al.*, 2003; James *et al.*, 2003; Karbowski and Youle, 2003; Lee *et al.*, 2004; Gomez-Lazaro *et al.*, 2008a).

The knowledge of upstream modulators of mitochondrial dynamics is still not complete. Mitochondrial fission is a highly regulated process mediated by a defined set of protein factors (Otsuga *et al.*, 1998; Mozdy *et al.*, 2000; Cerveny *et al.*, 2001; Karbowski *et al.*, 2004). One of these proteins, dynamin-related protein 1 (Drp1) in mammals, is a member of the dynamin family of large GTPases and mediates the scission of mitochondrial membranes through GTP hydrolysis. Drp1 is predominantly a cytoplasmic protein that associates with mitochondrial fission sites upon oligomerization (Labrousse *et al.*, 1999; Legesse-Miller *et al.*, 2003). In addition, Drp1 and the pro-apoptotic Bax protein have been co-localized to scission sites on mitochondria, suggesting that the mitochondrial fission machinery cooperates with the cell death machinery (Karbowski *et al.*, 2002).

Consistent with this, autophagy contributes to mitochondrial dysfunction-induced neurodegeneration (Puyal *et al.*, 2011) and *in vivo* administration of 3NP activates autophagy (Zhang *et al.*, 2009). How 3NP regulates autophagy, and how this is related to mitochondrial morphology is an important question. Therefore, in the present study, we investigated the contribution of the mitochondrial morphology pathway to autophagy activation as induced by 3NP. Our data show that 5 mM 3NP induced autophagy and resulted in mitochondrial changes. The mitochondrial morphology changed from elongated, tubular, interconnected structures to disintegrated punctate structures, due to an irreversible mitochondrial swelling. The 3NP effect was inhibited by the MPTP inhibitor cyclosporin A (CsA) but was independent of the molecular fission machinery, as revealed by the use of the Drp1 inhibitor, Mdivi-1. The participation of the Bax protein and ROS was also addressed.

Methods

Cell culture and drug treatment procedures

SH-SY5Y cell lines were obtained from the American Type Culture Collection (ATCC), and mouse embryonic fibroblasts (MEFs) (WT, $Bax^{-/-}$) were kindly provided by Dr M Serrano, (CNIO, Spain). Cell cultures were grown as described previously (Jordan *et al.*, 2004) in DMEM-F12 supplemented with 2 mM L-glutamine, 20 units·mL^{-1} penicillin-streptomycin, 5 mg·mL^{-1} gentamicin and 15% (v/v) FBS. Cells were grown in a humidified cell incubator at 37°C under a 5% CO_2 atmosphere. Cells were plated 24 h before transfection at a density of 5.3×10^4 cells cm^{-2}, on 35 mm μ-dish (Ibidi GmbH, Munich, Germany). 3NP was added to culture medium at a final concentration of 5 mM. Duration of pretreatment with TEMPOL (0.2 μM) and MnTBAP (10 nM) was 30 min.

Transfections

Twenty-four hours before transfection, cells were plated at a density of 5.3×10^4 cells cm^{-2} on poly-L-lysine-coated glass

slides. Transfection was achieved using Lipofectamine 2000 reagent (Invitrogen, Carlsbad, CA, USA) according to the manufacturer's protocol. Cells were transfected with the following plasmids encoding pDsRed2, Drp1-GFP and Bax-GFP. After 4 h of incubation, the transfection mixture was removed and replaced with fresh complete medium. The experiments were performed 24 h after transfection to allow protein expression.

Cell fixation, chromatin state and cell viability

Cells were fixed with 4% paraformaldehyde in PBS and 5% glucose-sucrose in PBS for 20 min at 37°C and washed three times with PBS. For assessment of chromatin state, the SH-SY5Y cells were plated on poly-L-lysine-coated glass slides. Nuclei were stained with Hoechst 33342 (0.5 mg·mL^{-1}) at RT for 5 min. Uniformly stained nuclei were scored as healthy, viable cells. Condensed or fragmented nuclei were scored as apoptotic. Cell viability after 3NP addition was assessed by measurement of LDH activity according to the protocol provided by the manufacturer (Promega, Madison, WI, USA). Briefly, the reaction mixture was added to conditioned media and removed from 24-well plates after centrifugation at 250× *g* for 10 min. After 30 min of incubation at room temperature, absorbance of samples at 490 nm was measured in a microplate reader (Bio-Rad, Hercules, CA, USA).

Image acquisition and processing

Micrographs were processed with Huygens Deconvolution Software (Scientific Volume Imaging, Hilversum, The Netherlands) and Adobe Photoshop. For quantitative analysis of mitochondrial morphology, the three patterns of mitochondrial morphology (filamentous, punctuate or intermediate) were recorded in at least 100 cells per coverslip observed on adjacent fields at magnification 63×. We assessed the robustness of this classification by comparing the proportions obtained with separate coverslips from the same experiment and from successive passages, as well as the proportions obtained by two independent examiners on three different cultures. The proportions observed were similar in all these experiments demonstrating that mitochondrial morphology could be reliably analysed and did not vary within and between experiments under basal culture conditions. Morphology was assessed by an examiner, unaware of the treatment administered.

Mitochondrial isolation

All animal care and experimental procedures complied with the Guiding Principles for Research Involving Animals and Human Beings of the American Physiological Society, the Guidelines of the European Union Council (86/609/CEE) and the Spanish regulations (BOE 67/8509-12, 1988) for the use of laboratory animals, and were approved by the Scientific Committee of the University of Castilla-La Mancha. All studies involving animals are reported in accordance with the ARRIVE guidelines for reporting experiments involving animals (McGrath *et al.*, 2010). A total of 4 rats were used in the experiments described here. All animals were housed at 22°C with 12 h light/12 h dark cycles and with full access to water and food. Liver mitochondria were isolated from adult male Wistar rats (300–350 g). Rat livers were homogenized with an automatic homogenizer (Heidolph®, Heidolph Instruments GmbH & Co., Schwabach, Germany). in a buffer containing 210 mM mannitol, 70 mM sucrose,1.0 mM EGTA, 0,1% BSA and 5 mM HEPES, pH 7.40, using 4 mL of medium per gram of tissue. Subsequently, differential centrifugation was applied. Briefly, the homogenate was centrifuged at 1000× *g* for 10 min and the supernatant at 10 000 × *g* for 10 min to precipitate mitochondria that were washed under the same conditions. The mitochondrial suspensions thus obtained (about 40 mg protein mL^{-1}) were used immediately after isolation.

Permeability transition pore activity in isolated mitochondria

Permeability transition pore opening was assayed spectrophotometrically as previously described (Galindo *et al.*, 2003). Specifically, mitochondria were suspended in 200 mL of solution containing 125 mM KCl, 20 mM HEPES, 2 mM KH_2PO_4, 1 mM EGTA, 1 mM $MgCl_2$, 5 mM malate and 5 mM glutamate with the pH adjusted to 7.08 with KOH to yield a final protein concentration of 1 mg·mL^{-1}. Changes in absorbance at 540 nm (A_{540}), indicating mitochondrial swelling as a result of MPTP opening, were determined after addition of different compounds using a microtitre plate reader (Bio-Rad, Hercules, CA, USA). Minor differences in the loading of the wells were normalized by presenting the values measured at a given time as the fraction of the initial A_{540} absorbance (~0.8).

Detection of mitochondrial permeability transition pore (MPTP) using calcein fluorescence

To demonstrate induction of the MPTPs, calcein fluorescence studies were carried out following the method of Petronilli *et al.* (1999). This method allows the direct visualization of permeability changes in mitochondria *in situ* (Perez-Alvarez *et al.*, 2010). Calcein/acetoxymethyl ester enters the cells and becomes fluorescent upon de-esterification. Co-loading of cells with cobalt chloride quenches the fluorescence in the cell, except in mitochondria, because mitochondrial membranes are impermeable to cobalt. However, during induction of the MPTPs, cobalt enters mitochondria and is able to quench the mitochondrial calcein fluorescence. Cultures were washed in Krebs–HEPES (K-H) buffer with the following ionic composition (in mol·L^{-1}): NaCl 140, KCl 5.9, $MgCl_2$ 1.2, HEPES 15, glucose 10 and $CaCl_2$ 2.5, pH 7.4, and incubated in fresh K–H containing calcein/acetoxymethyl ester (1 μM) and cobalt chloride (1 mM) for 30 min at 22–25°C. Following cobalt quenching, cultures were washed with K–H buffer, and images were collected with a confocal microscope within 5 min. This method was validated in cultured SH-SY5Y cells by the addition of 500 μmol·L^{-1} $CaCl_2$ along with the calcium ionophore A23187 (3 μmol·L^{-1}), which was pre-loaded with calcein and Co^{2+}. The addition of calcium caused a significant decrease in the mitochondrial calcein fluorescence in a time-dependent manner.

Mitochondrial potential

The effects of 3NP treatment on the mitochondrial potential (ΔΨ) in intact SH-SY5Y cells were determined in cells that were loaded with the ΔΨ-sensitive probe tetramethylrhodam-

ine methyl ester (TMRM). Briefly, SH-SY5Y cells were loaded with 10 nM TMRM for 10 min, washed with a standard external medium and challenged with 5 mM 3NP. Images were collected with a confocal microscope each 15 min during 180 min. Further details have been reported previously (Garcia-Martinez *et al.*, 2010).

Preparation of cytosolic and mitochondrial fractions

Cells were washed with ice-cold PBS, left on ice for 10 min and then re-suspended in isotonic homogenization buffer (250 mM sucrose, 10 mM KCl, 1.5 mM $MgCl_2$, 1 mM sodium-EDTA, 1 mM sodium-EGTA, 1 mM dithiothreitol, 0.1 mM PMSF and 10 mM Tris–HCl, pH 7.4) containing a proteinase inhibitor mixture (Roche, Basel, Switzerland). After 40 strokes in a Dounce homogenizer, the unbroken cells were spun down at 30× *g* for 5 min. The mitochondria fractions were fractionated at 750 g for 10 min and 14 000×*g* for 20 min, respectively, and separated from the supernatant (cytosolic fraction).

Western blotting

The protein concentration from each condition was quantified spectrophotometrically (Micro BCA Protein Reagent Kit, Pierce), and an equal amount of protein (30 μg) was loaded onto 10% SDS-PAGE gels. After electrophoresis, proteins were transferred to PVDF membranes (Immobilon; Millipore Corporation, Billerica, MA, USA). Non-specific protein binding was blocked with Blotto [4% w/v nonfat dried milk, 4% BSA (Sigma), and 0.1% Tween 20 (Sigma)] in PBS for 1 h. The membranes were incubated with a 1:1000 dilution of rabbit polyclonal anti-Bax antiserum (Cell Signalling, Beverly, MA, USA), anti-cytochrome C oxidase subunit IV (COX-IV; BD Biosciences, San José, CA, USA) or a 1:1000 dilution of a mouse anti-Drp1 monoclonal antibody (BD Biosciences) overnight at 4°C. After washing with Blotto, the membranes were incubated with peroxidase-labelled anti-mouse or anti-rabbit secondary antibodies (Promega) in Blotto. The signal was detected using an enhanced chemiluminescence detection kit (GE Healthcare, Little Chalfont, Buckinghamshire, UK). Immunoblots were developed by exposure to X-ray film (Eastman Kodak, Rochester, NY, USA). Band intensity was estimated densitometrically on a GS-800 calibrated densitometer (Bio-Rad Quantity One, Hercules, CA, USA).

Intracellular generation of ROS

The oxidation-sensitive fluorescent dye 2′,7′-dichlorodihydrofluorescein diacetate (DCFH-DA) was used to measure the production of ROS, mainly hydrogen peroxide and hydroxyl radicals, as previously described (Fernandez-Gomez *et al.*, 2005). This non-fluorescent ester is converted by ROS into DCF, which can easily be visualized by strong fluorescence at 530 nm when excited at 485 nm. Cells seeded in 96-well culture plates were incubated with DCFH-DA (10 μg·mL^{-1}) for 15 min, before adding either 3NP or vehicle and 30 min later fluorescence intensity was measured in a Spectra Max Gemini XS (Molecular Devices, Sunnyvale, CA, USA). The average relative percentage of ROS production in four wells from at least three separate cultures was determined.

Statistics

Data shown are means ± SEM, unless otherwise stated. Statistical significance of differences between groups was determined by ANOVA followed by a Newman–Keul's *post hoc* analysis. The level of statistical significance was set at $P < 0.05$.

Materials

DMEM-F12, penicillin-streptomycin, gentamicin and FBS were purchased from Gibco-Invitrogen (Carlsbad, CA, USA). The LDH kit (Citotox 96) is from Promega (Madison, WI, USA); poly-l-lysine, 3NP, Mdivi-1, Hoechst 33342 were obtained from Sigma-Aldrich (St. Louis, MO, USA). Mn(II-I)tetrakis (4-benzoic acid)porphyrin chloride (MnTBAP) and 4-hydroxy-2,2,6,6-tetramethylpiperidine-N-oxyl (TEMPOL) were purchased from Calbiochem (Darmstadt, Germany); the BCA protein assay kit from Pierce (Rockford, IL, USA). The pDsRed2-mito vector was provided by Clontech (Mountain View, CA, USA), Drp1-GFP was provided by T Wilson and Dr S Strack (Department Pharmacology, University of Iowa Carver College of Medicine), and GFP-Bax was a gift from Dr JHM Prehn (Department of Physiology and RCSI Neuroscience Research Centre, Royal College of Surgeons, Ireland). The stock solutions of 3NP (5 M in PBS), TEMPOL (0.2 μM in DMSO) and MnTBAP (10 nM in DMSO) were stored at –20°C.

Results

3NP induces autophagy in SH-SY5Y cells

The protein LC3 has been used as a specific marker for the quantification of autophagosomes. Overexpression of GFP-LC3 is a well-accepted, straightforward and specific assessment of autophagosome formation. SH-SY5Y cells were transfected with GFP-LC3 and kept for 24 h before treatment with 3NP. When these cells are cultured in regular DMEM medium supplemented with 10% FBS, only a small number of GFP-LC3 dots were detected (4 ± 0.2 per cell) (Figure 1A, C), and the chimeric protein was homogeneously distributed within the cytosol. The number of these LC3-GFP dots increased to 17 ± 1.2 per cell after 3 h treatment with 5 mM 3NP (Figure 1B, C). Cells with more than five autophagosomes were counted as autophagic cells. The number of autophagic cells in untreated conditions was about 16%, whereas in the presence of 3NP, this number increased to 85 % (Figure 1D).

3NP disrupts mitochondrial morphology

To study the mitochondrial morphology, SH-SY5Y cells were transfected with pDsRed2-mito plasmid to express the mitochondrial DsRed2 protein. After 24 h of transfection, untreated cultures present mitochondria with a long and tubular morphology (Figure 2A), which became dramatically shorter and rounder in response to 3 h of treatment with 5 mM 3NP (Figure 2B). Cell counting of the different mitochondrial morphologies (filamentous, mixed and fragmented) indicated that 3NP induced mitochondrial fragmentation and the formation of swollen, ball-shaped mitochondria in about 40% of the cells (Figure 2C). These changes in shape took place during the first hour of treatment because, when we examined the effect of a short-term (1 h) exposure to 3NP by replacing the culture medium with fresh medium lacking inhibitor and then examining the mitochondrial morphology, the morphological changes were not reversed (Figure 2D).

To examine if a collapse of the mitochondrial transmembrane potential accompanies mitochondrial fragmentation,

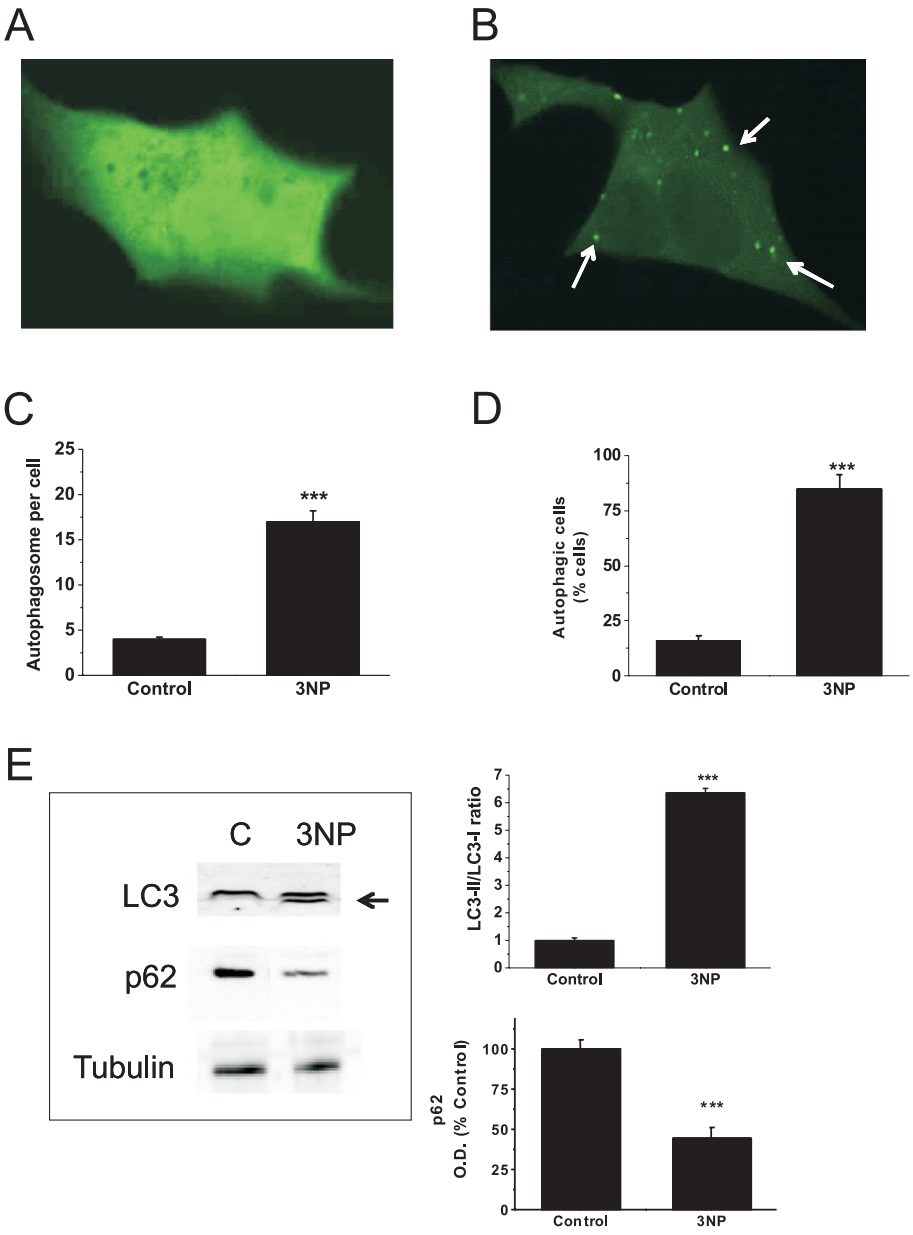

Figure 1

3NP induces autophagy. (A–B) Confocal images of SH-SY5Y cells 24 h after transfection with the LC3-GFP vector. Representative non-treated cells (control, A) or incubated for 3 h in 5 mM 3NP (B). Scale bar, 10 μm. (C) Number of cytosolic LC3-GFP vacuoles per cell were determined in at least six different cultures under basal conditions (control) and after 3 h treatment with 5 mM 3NP. (D) Proportions of autophagic cells in cell cultures challenged or not with 5 mM 3NP cells for 3 h. Data represent mean ± SEM of four independent experiments (***$P < 0.001$, significantly different from Control, *t*-test. (E) Left representative Western blot showing LC3-I and II; p62 and tubulin protein bands from total cellular extracts of SH-SY5Y cells challenged or not with 5 mM 3NP for 3 h. Histograms: Quantitative analysis of the ratio of LC3II to LC3I ($n = 4$) and (lower graph) of p62 levels normalized to tubulin ($n = 4$). Results are expressed as mean ± SEM ($n = 5$). ***$P < 0.001$, significantly different from Control, *t*-test.

SH-SY5Y cells were incubated with TMRM, a fluorescent dye that accumulates rapidly and selectively within mitochondria. Uptake of TMRM depends on and is directly proportional to the membrane potential. Statistical analysis of the TMRM fluorescence intensity showed differences between controls and cells treated with 5 mM 3NP, after 45 min of treatment (36 ± 2.3% of TMRM fluorescence level of controls, $P < 0.01$, $n = 5$).

Furthermore, these events took place before the appearance of any marker of cell death. After 3 h, cells kept the capacity to retain LDH intracellularly (Figure 2E, 3 h of total treatment time). But, consistent with the well-known toxicity of this inhibitor and the fact that we were using toxic concentrations, cell cultures lost viability when they were cultured for an additional 21 h (Figure 2E; 24 h of total treatment time).

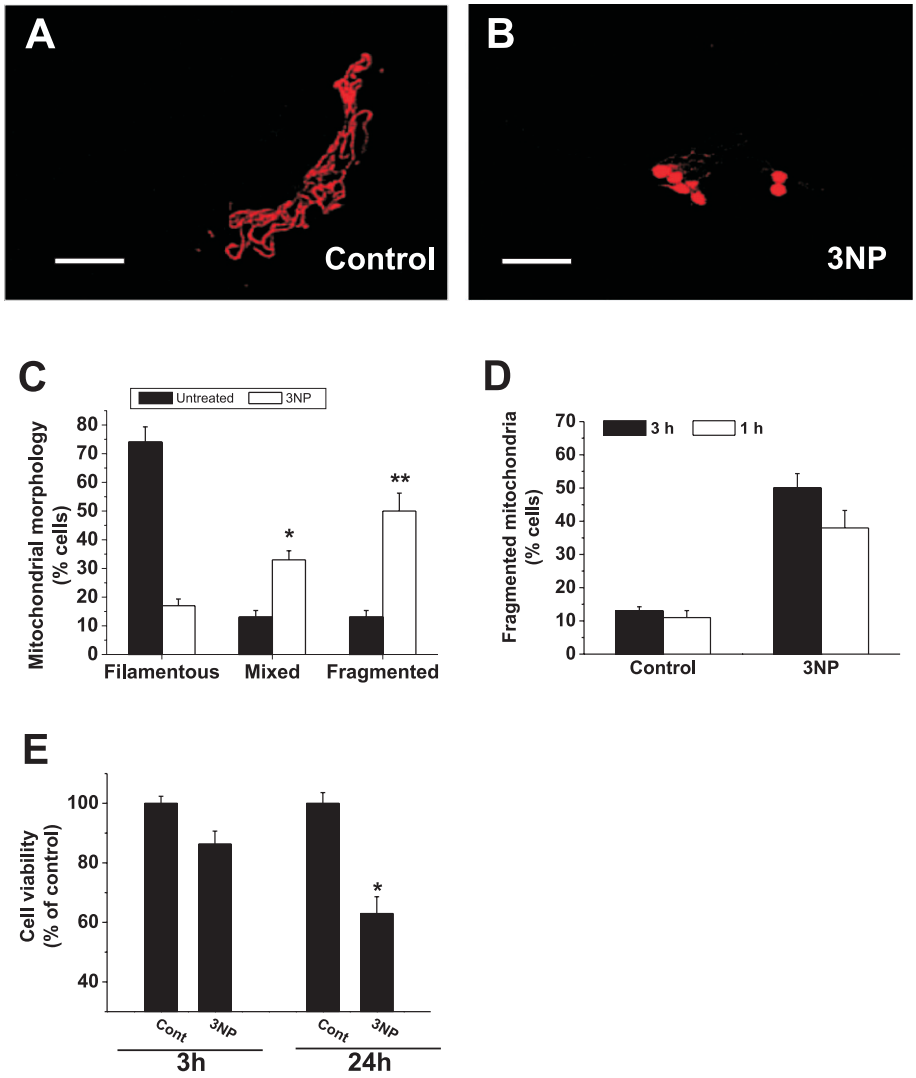

Figure 2

3NP disrupts mitochondrial morphology. (A–B) Confocal images of SH-SY5Y cells 24 h after transfection with the pDsRed2-mito vector. Representative mitochondrial morphology in non-treated cells (control, A) or incubated for 3 h in 5 mM 3NP (B). Scale bar, 10 μm. (C) Proportions of cells with filamentous, mixed or fragmented mitochondrial patterns were determined in at least six different cultures under basal conditions (untreated) and after 3 h treatment with 5 mM 3NP (*$P < 0.05$, significant effects of 3NP, *t*-test. (D) 3NP does not induce reversible morphological changes. Proportions of cells with fragmented mitochondrial patterns were determined after 3 h (untreated), or 1 h and 2 h after removal of the inhibitor from cell cultures challenged for 1 h with 3NP. (E) Cell viability studies of cell cultures that were exposed for 3 or 24 h to 5 mM 3NP. Data represent mean ± SEM of four independent experiments *$P < 0.05$, significantly different as indicated, *t*-test.

Mitochondrial permeability transition pore (MPTP) formation due to 3NP

Under certain conditions, mitochondria respond to cytotoxic stimuli by forming MPTPs. This results in the swelling of the organelle (Crompton, 1999). First, we used the calcein staining/Co^{2+}-quenching technique to image the formation of MPTPs. Confocal microscopy analysis revealed that as early as 30 min after 5 mM 3NP addition, a decrease in mitochondrial calcein fluorescence was evident (Figure 3A–E). To elucidate if this phenomenon was due to a direct effect on mitochondria, we isolated mitochondria from rat livers and measured changes in absorbance at 540 mm, which is an indicator of organelle swelling. 3NP induced a significant decrease in the A_{540} (Figure 3F), indicating that exposure to 3NP induced mitochondrial swelling. The role of MPTP formation on 3NP-induced autophagy was then assessed. Cell cultures were pre-treated for 30 min with the MPTP inhibitor CsA (1 μM) and then challenged with 5 mM 3NP. The inhibition of MPTP blocked 3NP-induced autophagy (24.6 ± 2.4% autophagic cells in the presence of CsA vs. 84.6 ± 5.4% in the absence of CsA; $P < 0.001$, $n = 5$ independent cultures). Furthermore, CsA prevented the mitochondrial changes induced by 3NP (Figure 4D).

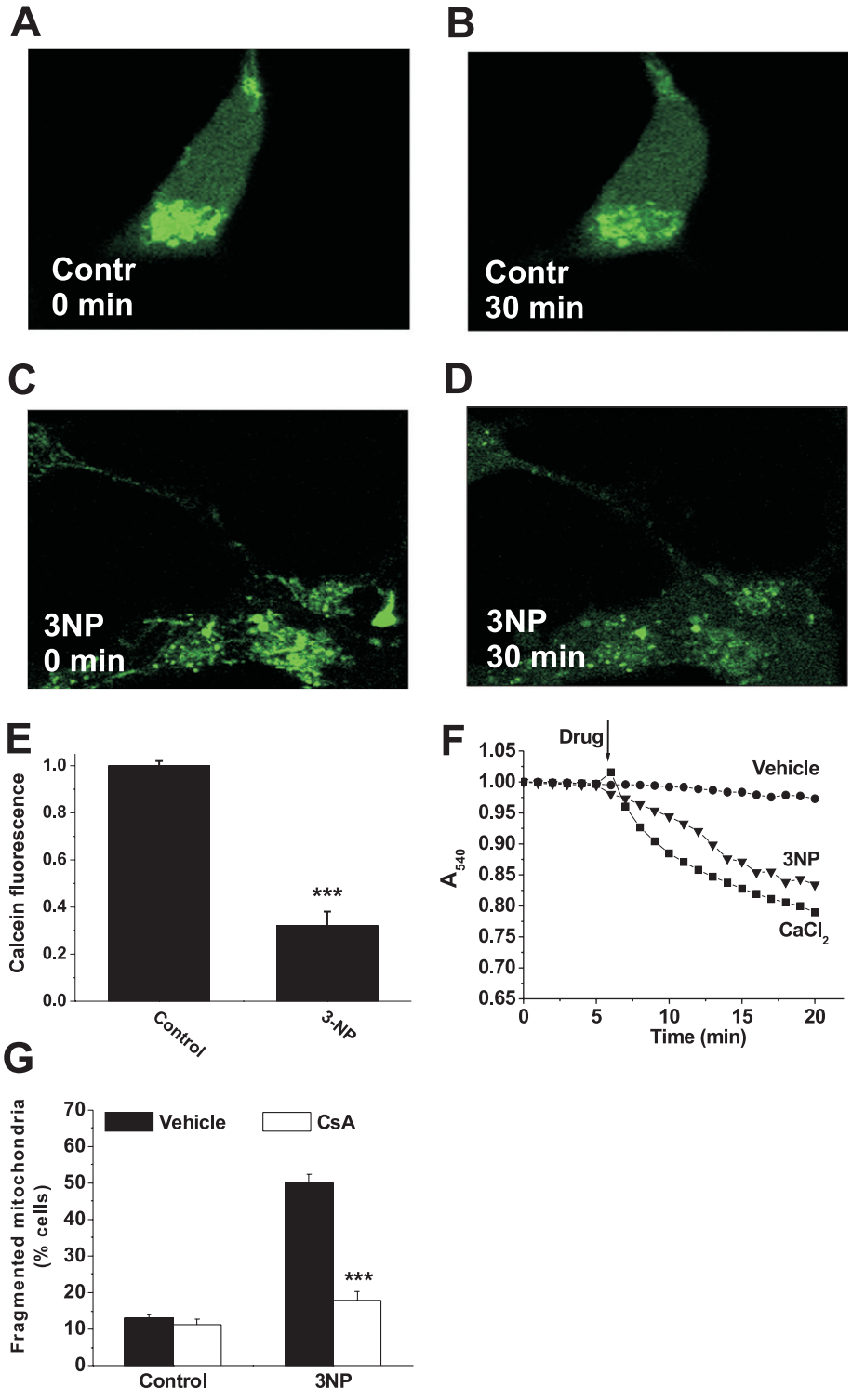

Figure 3

MPTP participation in 3NP-induced mitochondrial alteration. (A–D) Changes in mitochondrial fluorescence of calcein. SH-SY5Y cells loaded with calcein/Co^{2+} were treated with 5 mM 3NP. Representative confocal images of calcein fluorescence in SH-SY5Y cells, before (left) or 30 min after (right) treatment. (E) Fluorescence intensity normalized to the initial value. Data represent mean ± SEM of four independent experiments. (F) 3NP induces mitochondrial swelling. Mitochondrial suspensions were exposed to 5 mM 3NP, and A_{540} was recorded. Ca^{2+} (75 μM) was used as a positive control for mitochondrial swelling. Data represent mean ± SEM of four independent experiments. ***P< 0.001 significantly different from vehicle, *t*-test.

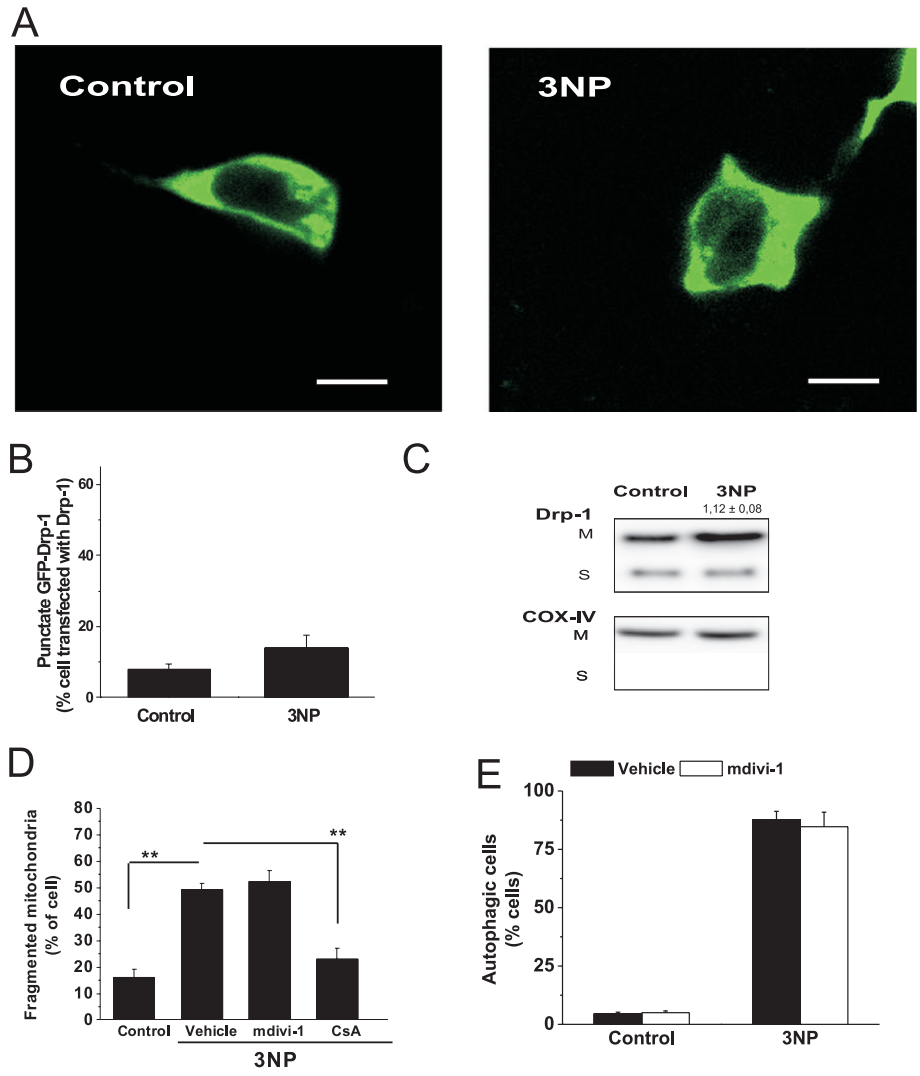

Figure 4

Drp1 displays cytosolic localization after 3NP treatment. (A) Confocal imaging of SH-SY5Y cells transfected with Drp1-GFP and treated with 5 mM 3NP. Drp1-GFP demonstrated primarily diffuse staining in control (left) and after 3 h treatment with 3NP (right). Images shown are representative of four separate experiments, each performed in triplicate. (B) Number of cells with punctuate Drp1-GFP distribution were counted and expressed as percentage of the total number of cells expressing Drp1-GFP. Data shown are the mean ± SEM. of at least three experiments, each performed in triplicate. (C**)** Levels of Drp1 were determined in mitochondrial fraction (M) and soluble extracts (S) from SH-SY5Y control cells and cells treated with 5 mM 3NP. COX-IV protein levels (lower panel) were used as an index of mitochondrial contamination. Equal amounts of protein (30 µg/lane) were loaded onto the gels. The immunoblots shown are representative of three independent experiments. Fold variation of Drp1 levels normalized to COX are shown at the bottom of each line. Data shown are mean ± SEM (n = 5). (D) Effects of Mdivi-1 and CsA on 3NP-induced changes in mitochondrial morphology. SH-SY5Y cells transfected with pDsRed2-mito vector were co-treated with either 10 µM Mdivi-1 or CsA and 5 mM 3NP. Proportions of cells with filamentous, mixed or fragmented mitochondrial patterns were determined in at least six different cultures under basal conditions (control) and after 3 h treatment with 5 mM 3NP. $^{**}P < 0.01$, significantly different as indicated, one-way ANOVA with Tukey's *post hoc* test. (E)Mdivi-1 effects on 3NP-induced autophagy. SH-SY5Y cells transfected with LC3-GFP vector and co-treated with 10 µM Mdivi-1 and 5 mM 3NP. Proportions of autophagic cells in cell cultures challenged or not with 5 mM 3NP cells for 3 h. Data shown are the mean ± SEM of four independent experiments.

3NP did not activate mitochondrial Drp1 translocation

Translocation of the cytosolic protein Drp1 to the mitochondria has been associated with mitochondrial fission. To evaluate the effects of 3NP on Drp1 cellular localization, cell cultures overexpressing Drp1-GFP were used. In untreated cultures, Drp1-GFP distribution was cytosolic (Figure 4A). Treatment of the cells with 3NP (5 mM, 3 h) did not induce changes in Drp1-GFP distribution (Figure 4B). We also assayed the localization of this protein using immunoblotting of cellular subfractions isolated from cell cultures. Consistent with the above results, 3NP did not induce the translocation of Drp1 from the cytosol to the mitochondria (Figure 4C).

To evaluate the role of Drp1 in 3NP-induced autophagy, the mitochondrial division inhibitor Mdivi-1 was used (Cassidy-Stone *et al.*, 2008; Tanaka and Youle, 2008). Cell cultures were pre-treated for 30 min with Mdivi-1 (10 μM) before being challenged with 5 mM 3NP. Furthermore, Mdivi-1 (10 μM) treatment resulted in extensive budding and elongation of the mitochondrial network, but did not inhibit the mitochondrial fragmentation caused by 3NP (Figure 4D). Furthermore, the inhibition of Drp1 did not block 3NP-induced autophagy (Figure 4E).

Bax translocates to the mitochondria after 3NP addition

Bax is a pro-apoptotic protein that participates in cell death and mitochondrial fission. To study whether the 3NP treatment induced Bax translocation, we analysed cells overexpressing GFP-Bax and performed immunoblotting of cellular subfractions isolated from cell cultures. As shown in Figure 5, both approaches revealed translocation of Bax to the mitochondria in cell cultures challenged with 5 mM 3NP. 3NP induced an increase in the number of cells with a punctuate distribution of Bax-GFP (Figure 5A–C), and immunoblotting revealed an increase of the levels of the protein in the cytosol (S, Figure 5C) as well as in mitochondrial subfractions (M, Figure 5C).

To investigate if inhibition of Drp1 modulated the translocation of Bax to the mitochondria, SH-SY5Y cells transfected Bax-GFP were co-treated with Mdivi-1 and 3NP. After 3 h, the number of cells with Bax-GFP punctuated distribution was determined. As shown in Figure 5D, 10 μM Mdivi-1 failed to affect 3NP-induced Bax-GFP translocation to mitochondria.

Next, we aimed to elucidate the role of Bax protein in 3NP-induced mitochondrial morphology alterations. To this end, we used embryonic fibroblasts from $Bax^{-/-}$ mice. Lack of Bax protein expression neither prevented 3NP-induced MPTP formation, evaluated after 45 min of 3NP treatment using a confocal microscopy calcein technique (Figure 5E), nor did it affect the alterations in mitochondrial morphology, measured 3 h later (Figure 5F).

Role of ROS

To further delineate the physiological consequences of 3NP addition, we also considered the role of ROS. In this study, we used DCFH-DA, a redox-sensitive probe, to demonstrate if 3NP increased intracellular levels of ROS. After 3 h of treatment, we found that cells challenged with 3NP displayed a significant increase in DFA fluorescence emission intensity (Figure 6A, vehicle). Next, we determined the effect of ROS scavenger drugs on 3NP-induced effects. Cells were pre-incubated with the antioxidants TEMPOL (0.2 μM) or MnTBAP (10 nM) 30 min before 3NP treatments. Confocal microscopy analysis of cell cultures overexpressing LC3-GFP protein revealed that both scavengers failed to inhibit the formation of autophagic cells by 3NP (Figure 6B). Furthermore, both these drugs failed to prevent 3NP-induced changes in mitochondrial morphology (Figure 6C).

Finally, we assessed the relationship between changes in mitochondrial morphology and 3NP-induced ROS by pre-treating cell cultures with either Mdivi-1 or CsA and measuring ROS production 3 h after 3NP addition. As shown in Figure 6A, only 1 μM CsA, but not Mdivi-1, was able to block 3NP-induced ROS production.

Discussion

In this study, SH-SY5Y cells were used to investigate the effect of 3NP on autophagy and its relationship with alterations in mitochondrial morphology. We demonstrated that 3NP provoked autophagy through irreversible mitochondrial changes. This involved organelle swelling by the formation of MPTPs rather than activation of the fission program.

Autophagy is emerging as a pathway relevant to physiology and alterations in this process contribute to several diseases (Kroemer and Levine, 2008). At 3 h after addition of 5 mM 3NP, SY-SY5Y cell cultures presented an increased number of autophagosomes, which is characteristic of autophagy. Consistent with this observation, morphological and biochemical analyses of rat striatum treated with 3NP by stereotaxic injection showed activation of autophagy in striatal cells (Zhang *et al.*, 2009). By this time point, cell cultures exposed to 3NP showed clear changes in mitochondrial morphology, but not clear signs of cell death. The organelles presented a markedly shorter and rounder morphology, compared with those from untreated cultures. To observe this we used a fluorescent protein, pDsRed2-mito, targeted to the mitochondria. pDsRed2-mito is efficiently localized to both wild-type and respiratory-deficient mitochondria, allowing studies of mitochondrial morphology in compromised conditions such as the addition of 3NP, well-known to inhibit complex II. Although we mostly evaluated morphological alterations at 3 h after 3NP addition, mitochondrial alterations take place during the early stages of treatment. In preliminary studies, we were able to detect mitochondria with altered morphology as early as 1 h after 3NP addition. Moreover, if we treated cells only for 1 h and analysed the mitochondrial morphology 3 h later, the effects on mitochondrial morphology were similar to those seen after 3h exposure to 3NP. However, these effects could be a consequence of non-reversible inhibition of complex II by 3NP. On the other hand, supporting our hypothesis are the data from the analysis of MPTP formation both *in vivo* and in isolated mitochondria.

The influence of mitochondrial dynamics on cellular functioning is perhaps best appreciated in neurons, as these cells have a high energy requirement to support distantly located and metabolically demanding synaptic terminals. Strong evidence has been presented, indicating that mitochondrial malfunction plays a crucial part in the pathogenesis of Huntington's disease. Mitochondria isolated from lymphocytes of Huntington's disease patients have decreased Ca^{2+}-buffering capacity Moreover, possibly due to a direct interaction between the poly-glutamine stretch in mutant huntingtin and the mitochondria, their mitochondrial membrane potential depolarizes earlier at lower Ca^{2+} concentrations (Panov *et al.*, 2002).

We observed depletion in calcein fluorescence during the first 30 min after 3NP addition. In isolated mitochondria, 3NP induced mitochondrial swelling by CsA-sensitive classic MPTP formation. Consistent with This observation was consistent with that of Nishimura *et al.* (2008) who described how 3NP-induced functional changes of mitochondria were

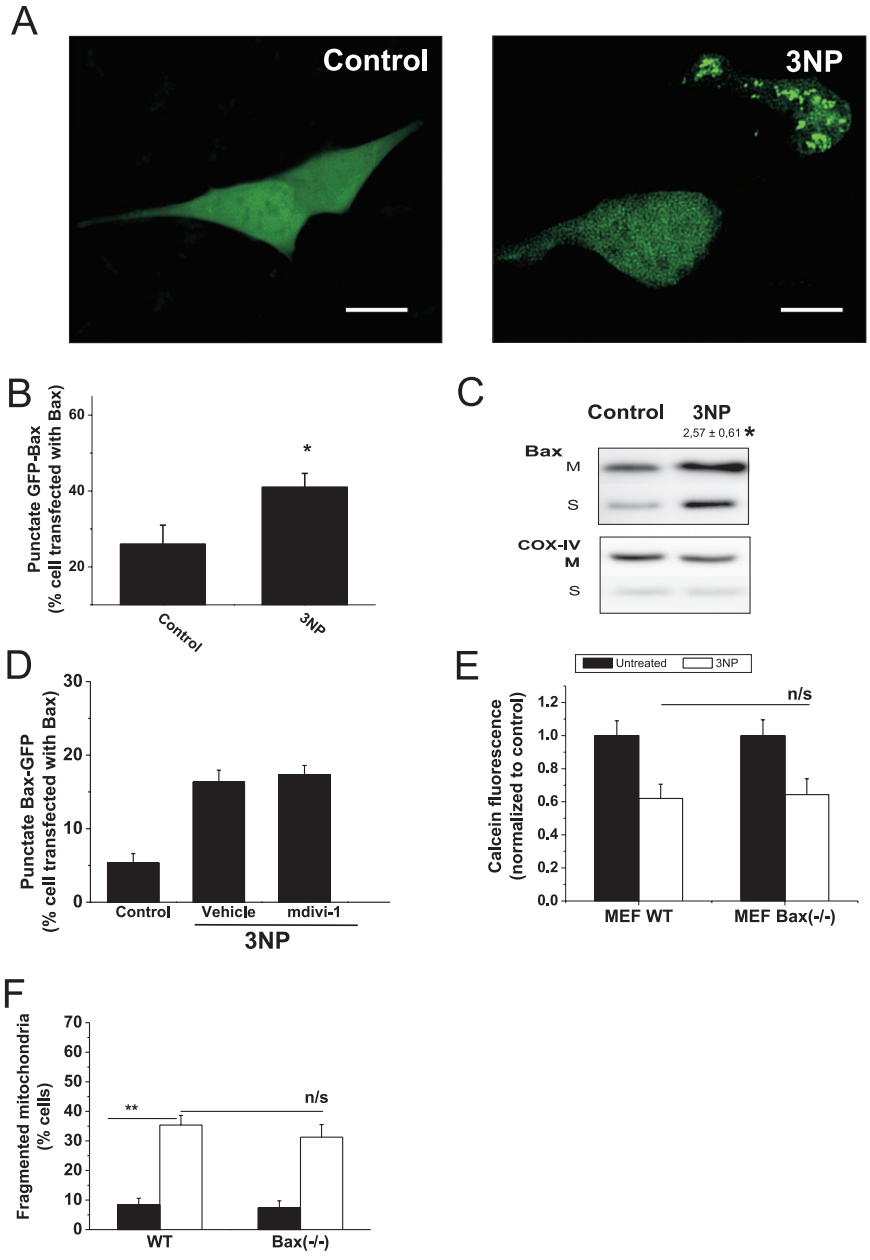

Figure 5

3NP induces Bax translocation to the mitochondria but does not mediate alterations in mitochondrial morphology. (A) Confocal imaging of SH-SY5Y cells that were transfected with Bax-GFP, incubated for 24 h to allow sufficient Bax-GFP expression and treated with 5 mM 3NP. After 3 h exposure the cells were fixed in 4% paraformaldehyde, and confocal images were captured using a 63× oil immersion lens. Bax-GFP demonstrated primarily diffuse staining in control (left), whereas 3 h after 3NP treatment a punctuate pattern is evident. Images shown are representative of four separate experiments, each performed in triplicate. (B) The numbers of cells with punctuate Bax-GFP distribution were counted and expressed as percentage of the total number of cells. Data shown are the mean ± SEM of at least three experiments, each performed in triplicate. *$P < 0.05$, significantly different from control, *t*-test. (C) Levels of Bax were determined in mitochondrial fraction (M) and soluble extracts (S) from SH-SY5Y cells treated with or without 5 mM 3NP. COX-IV protein levels (lower panel) were used as an index of mitochondrial contamination. Equal amounts of protein (30 μg/lane) were loaded onto the gels. An immunoblot from SH-SY5Y cell cultures, representative of five independent experiments, is shown. Fold variation of Bax levels (mean ± SEM; $n = 5$) normalized to control, are shown at the top of each line. . (D) Drp1 inhibition does not modify Bax-GFP translocation. SH-SY5Y cells transfected with Bax-GFP plasmid were co-treated with 10 μM Mdivi-1 and with 5 mM 3NP. After 3 h of treatment, proportions of cells with diffuse or punctuate GFP-distribution patterns were determined in at least six different cultures. Data represent mean ± SEM of four independent experiments. (E) Confocal calcein fluorescence intensity in MEF from Bax$^{-/-}$ mice 45 min after 5 mM 3NP treatments. Values were normalized to the initial value. Data represent mean ± SEM of four independent experiments. (F) MEF from Bax$^{-/-}$ mice were transfected with pDsRed2-mito vector and treated with 5 mM 3NP. Proportions of cells with fragmented mitochondrial patterns were determined in at least six different cultures under basal conditions (control) and after 3 h treatment with 5 mM 3NP (3NP, n/s $P > 0.05$; **$P < 0.01$, significantly different as indicated; one-way ANOVA with Tukey's *post hoc* test.

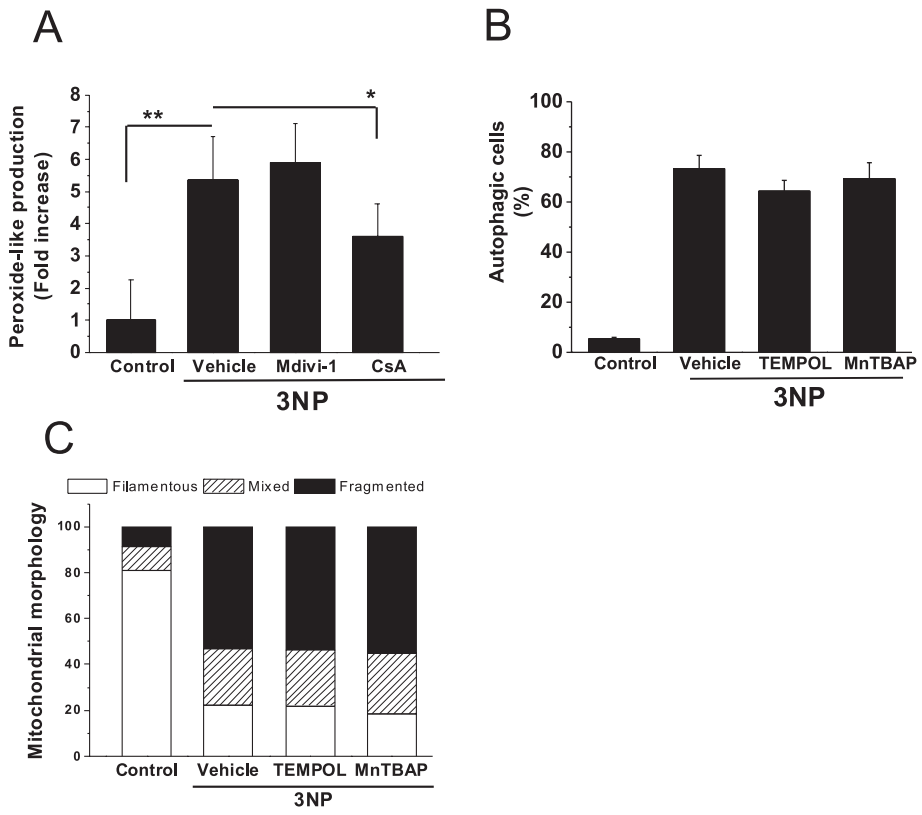

Figure 6

ROS do not function as second messengers in 3NP-induced mitochondrial fragmentation. (A) 3NP induces the production of peroxides. Cell cultures were pre-treated with 10 μM Mdivi-1, 1 μM CsA or vehicle for 30 min before the addition of 5 mM 3NP, and production of peroxide-like ROS was measured 3 h after 3NP addition. Data were normalized to vehicle-treated cells, and values shown are the mean ± SEM of five independent experiments performed in quadruplicate. *$P < 0.05$, **$P < 0.001$, significantly different as indicated, one-way ANOVA with Tukey's *post hoc* test; ns, $P > 0.05$). (B) TEMPOL (0.2 μM) or MnTBAP(10 nM) effects on 3NP-induced autophagy. SH-SY5Y cells were transfected with LC3-GFP vector and pre-incubated with 0.2 μM TEMPOL or 10 nM MnTBAP for 30 min prior to treatment with 5 mM 3NP. Proportions of autophagic cells in cell cultures that were challenged or not with 5 mM 3NP cells for 3 h. Data represent mean ± SEM of four independent experiments. (C) Confocal microscopy analysis of mitochondrial morphology of cell cultures overexpressing pDsRed2-mito protein and pre-incubated with 0.2 μM TEMPOL or 10 nM MnTBAP 30 min before treatment with 5 mM 3NP. Proportions of cells with filamentous, mixed or fragmented mitochondrial patterns were determined in at least six different cultures under basal conditions (control) and after 3 h of treatment with inhibitors. Data represent mean ± SEM of four independent experiments.

caused by the CsA-sensitive classic MPTP. Furthermore, Leventhal *et al*. (2000) showed that the neuroprotective properties of CsA are mediated by its ability to prevent MPTP opening during exposure to high levels of calcium or oxidative stress in 3NP-lesioned rats.

Our data support the notion that mitochondrial fission did not actively participate in the 3NP-induced morphological changes we observed. Mitochondrial fission requires Drp1, a large GTPase of the dynamin family. Drp1 is cytosolic but a subpool of the protein concentrates in discrete spots on mitochondria at sites of future fission (Labrousse *et al*., 1999; Legesse-Miller *et al*., 2003) and assembles into rings around mitochondria and constricts their membranes, breaking down the organelles in a GTP hydrolysis-dependent mechanism (Ingerman *et al*., 2005). In our study, 3NP did not recruit Drp1 to mitochondria. We reach this conclusion from several kinds of experiments that included assaying the levels of Drp1 protein in cytosolic and mitochondrial subcellular fractions, which failed to detect increases in either fraction. In addition, confocal microscopy of cell cultures overexpressing Drp1-GFP revealed that addition of 3NP did not modify the cytosolic and diffuse distribution of Drp1. A similar conclusion was reached when we analysed the capacity of 3NP to induce mitochondrial morphological alterations in cell cultures where Drp1 was inhibited using Mdivi-1. Mdivi-1 selectively inhibits the activity of mitochondrial division dynamin-related proteins by binding to an allosteric site that does not exclusively act through the GTPase domain (Cassidy-Stone *et al*., 2008). The concentration of Mdivi-1 used in our study (10 μM) was sufficient to inhibit Drp1 as was shown by extensive budding and elongation of the mitochondrial network in the SH-SY5Y cell cultures.

After 3NP addition, Bax translocated to the mitochondria in SH-SY5Y cells. The participation of Bax in mitochondrial fission is controversial (Antignani and Youle, 2006). Bax was found to co-localize with Drp1 and Mfn2 at mitochondrial fission sites in apoptotic cells (Karbowski *et al*., 2002) and has been suggested to participate directly in apoptotic mitochondrial fission. Consistent with this, Drp1 or Fis1 knockdown resulted in a reduced accumulation of Bax in mitochondria

(Lee *et al.*, 2004). However, in SH-SY5Y cells, Bax translocation occurred in a non-concatenate process of mitochondrial fission after 3NP treatment. Indeed, by the time that mitochondria were already fragmented (1–3 h), Bax had not yet translocated to the mitochondria. Moreover, and in support of a different activation route, 3NP-induced Bax translocation was not inhibited by Mdivi-1. Our observations were In agreement withealier studies in which Drp1 knockdown or a mutant Drp1K38A exhibited no effect on Bax dynamics (Frank *et al.*, 2001; Lee *et al.*, 2004). We have already shown, in a different neurodegenerative model using MEF cell cultures from mice lacking Bax, that this protein is not required for 6-OHDA-induced mitochondrial fragmentation (Gomez-Lazaro *et al.*, 2008a). Thus, the function of Bax might be related to MOMP in 3NP-treated cells. Consistent with this hypothesis, mitochondrial energization associated with apoptosis promotes Bax translocation to mitochondria (Smaili *et al.*, 2001; Gomez-Lazaro *et al.*, 2008b; Perez-Alvarez *et al.*, 2009), and we and others have found that Bax actively participates in neurodegenerative process (Gomez-Lazaro *et al.*, 2008b; Perez-Alvarez *et al.*, 2009). Indeed, 3NP, in striatal neurons, produced distribution of pro-apoptotic proteins including Bad and Bax (Galas *et al.*, 2004).

We also addressed the function of ROS in 3NP-activated pathways. Our data indicate that, although 3NP increased intracellular ROS, the ROS did not appear to be a significant signalling link between 3NP and the mitochondrial fragmentation machinery. When ROS were scavenged, a slight, non-significant, inhibition of autophagy and mitochondrial alteration was observed. However, ROS induction was blocked when we inhibited mitochondrial swelling using CsA. Again, and consistent with the notion that mitochondrial fission does not play a role in our model, Mdivi-1 did not modulate 3NP-induced ROS production. An explanation for this observation can be found in the results of Liot *et al.* (2009) who placed mitochondrial fragmentation upstream of ROS production. These authors observed that 3NP induced an initial wave of ROS formation, which was not related to mitochondrial fragmentation or cell death.

Our data show a direct correlation between MPTP formation and autophagy induced by 3NP treatment. Activation of autophagy preceded the apoptotic process and was mediated, at least partly, by ROS and MPTP formation. Further elucidation of beneficial and detrimental roles of autophagy in neurodegenerative diseases will shed new light on the pathogenesis of neurodegenerative diseases that involve mitochondrial dysfunction.

Acknowledgements

We thank Joaquín Soriano (UCLM) and Manuel Izquierdo (CISC) for advice on image acquisition and processing, Jose M Buendia, Noemi Pérez and Carlos Garrido for technical help, Antonio Ortega (CHUA) for help with illustrations, and T Wilson, Dr S Strack and Dr JHM Prehn for providing vectors. This work was supported by SAF2008-05143-C03-1 from Ministerio de Ciencia e Innovación and PI2007/55 Consejería de Sanidad from Junta de Comunidades de Castilla-La Mancha (to JJ) and by 'Incorporación de grupos emergentes' FIS CARLOS III (EMER07/023) and FIS-FEDER (PI080693) and PI11/00736 (to MFG). MES is a FIS-FEDER grant fellow.

Conflicts of interest

None.

References

Antignani A, Youle RJ (2006). How do Bax and Bak lead to permeabilization of the outer mitochondrial membrane? Curr Opin Cell Biol 18: 685–689.

Beal MF, Brouillet E, Jenkins BG, Ferrante RJ, Kowall NW, Miller JM, Storey E, Srivastava R, Rosen BR, Hyman BT (1993) Neurochemical and histological characterization of striatal excitotoxic lesions produced by mitochondrial toxin 3-nitropropionic acid. J Neurosci 13: 4181–4192.

Bossy-Wetzel E, Barsoum MJ, Godzik A, Schwarzenbacher R, Lipton SA (2003). Mitochondrial fission in apoptosis, neurodegeneration and aging. Curr Opin Cell Biol 15: 706–716.

Bove J, Prou D, Perier C, Przedborski S (2005). Toxin-induced models of Parkinson's disease. NeuroRx 2: 484–494.

Brouillet E, Conde F, Beal MF, Hantraye P (1999). Replicating Huntington's disease phenotype in experimental animals. Prog Neurobiol 59: 427–468.

Browne SE, Beal MF (2002) Toxin-induced mitochondrial dysfunction. Int Rev Neurobiol 53: 243–279.

Cassidy-Stone A, Chipuk JE, Ingerman E, Song C, Yoo C, Kuwana T *et al.* (2008). Chemical inhibition of the mitochondrial division dynamin reveals its role in Bax/Bak-dependent mitochondrial outer membrane permeabilization. Dev Cell 14: 193–204.

Cerveny KL, McCaffery JM, Jensen RE (2001). Division of mitochondria requires a novel DMN1-interacting protein, Net2p. Mol Biol Cell 12: 309–321.

Chipuk JE, Fisher JC, Dillon CP, Kriwacki RW, Kuwana T, Green DR (2008). Mechanism of apoptosis induction by inhibition of the anti-apoptotic BCL-2 proteins. Proc Natl Acad Sci USA 105: 20327–20332.

Crompton M (1999). The mitochondrial permeability transition pore and its role in cell death. Biochem J 341: 233–249.

Cuervo AM (2004). Autophagy: many paths to the same end. Mol Cell Biochem 263: 55–72.

Detmer SA, Chan DC (2007). Functions and dysfunctions of mitochondrial dynamics. Nat Rev Mol Cell Biol 8: 870–879.

Fernandez-Gomez FJ, Gomez-Lazaro M, Pastor D, Calvo S, Aguirre N, Galindo MF *et al.* (2005). Minocycline fails to protect cerebellar granular cell cultures against malonate-induced cell death. Neurobiol Dis 20: 384–391.

Ferreirinha F, Quattrini A, Pirozzi M, Valsecchi V, Dina G, Broccoli V *et al.* (2004). Axonal degeneration in paraplegin-deficient mice is associated with abnormal mitochondria and impairment of axonal transport. J Clin Invest 113: 231–242.

Frank S, Gaume B, Bergmann-Leitner ES, Leitner WW, Robert EG, Catez F *et al.* (2001). The role of dynamin-related protein 1, a mediator of mitochondrial fission, in apoptosis. Dev Cell 1: 515–525.

Galas MC, Bizat N, Cuvelier L, Bantubungi K, Brouillet E, Schiffmann SN *et al.* (2004). Death of cortical and striatal neurons induced by mitochondrial defect involves differential molecular mechanisms. Neurobiol Dis 15: 152–159.

Galindo MF, Jordan J, Gonzalez-Garcia C, Cena V (2003). Reactive oxygen species induce swelling and cytochrome c release but not transmembrane depolarization in isolated rat brain mitochondria. Br J Pharmacol 139: 797–804.

Garcia-Martinez EM, Sanz-Blasco S, Karachitos A, Bandez MJ, Fernandez-Gomez FJ, Perez-Alvarez S *et al.* (2010). Mitochondria and calcium flux as targets of neuroprotection caused by minocycline in cerebellar granule cells. Biochem Pharmacol 79: 239–250.

Gomez-Lazaro M, Bonekamp NA, Galindo MF, Jordan J, Schrader M (2008a). 6-Hydroxydopamine (6-OHDA) induces Drp1-dependent mitochondrial fragmentation in SH-SY5Y cells. Free Radic Biol Med 44: 1960–1969.

Gomez-Lazaro M, Galindo MF, Concannon CG, Segura MF, Fernandez-Gomez FJ, Llecha N *et al.* (2008b). 6-Hydroxydopamine activates the mitochondrial apoptosis pathway through p38 MAPK-mediated, p53-independent activation of Bax and PUMA. J Neurochem 104: 1599–1612.

Ingerman E, Perkins EM, Marino M, Mears JA, McCaffery JM, Hinshaw JE *et al.* (2005). Dnm1 forms spirals that are structurally tailored to fit mitochondria. J Cell Biol 170: 1021–1027.

James DI, Parone PA, Mattenberger Y, Martinou JC (2003). hFis1, a novel component of the mammalian mitochondrial fission machinery. J Biol Chem 278: 36373–36379.

Jordan J, Galindo MF, Tornero D, Gonzalez-Garcia C, Cena V (2004). Bcl-x L blocks mitochondrial multiple conductance channel activation and inhibits 6-OHDA-induced death in SH-SY5Y cells. J Neurochem 89: 124–133.

Karbowski M, Youle RJ (2003). Dynamics of mitochondrial morphology in healthy cells and during apoptosis. Cell Death Differ 10: 870–880.

Karbowski M, Lee YJ, Gaume B, Jeong SY, Frank S, Nechushtan A *et al.* (2002). Spatial and temporal association of Bax with mitochondrial fission sites, Drp1, and Mfn2 during apoptosis. J Cell Biol 159: 931–938.

Karbowski M, Jeong SY, Youle RJ (2004). Endophilin B1 is required for the maintenance of mitochondrial morphology. J Cell Biol 166: 1027–1039.

Kroemer G, Levine B (2008). Autophagic cell death: the story of a misnomer. Nat Rev Mol Cell Biol 9: 1004–1010.

Labrousse AM, Zappaterra MD, Rube DA, van der Bliek AM (1999). C. elegans dynamin-related protein DRP-1 controls severing of the mitochondrial outer membrane. Mol Cell 4: 815–826.

Leber B, Andrews DW (2010). Closing in on the link between apoptosis and autophagy. F1000 Biol Rep 2: 88.

Lee YJ, Jeong SY, Karbowski M, Smith CL, Youle RJ (2004). Roles of the mammalian mitochondrial fission and fusion mediators Fis1, Drp1, and Opa1 in apoptosis. Mol Biol Cell 15: 5001–5011.

Legesse-Miller A, Massol RH, Kirchhausen T (2003). Constriction and Dnm1p recruitment are distinct processes in mitochondrial fission. Mol Biol Cell 14: 1953–1963.

Leventhal L, Sortwell CE, Hanbury R, Collier TJ, Kordower JH, Palfi S (2000). Cyclosporin A protects striatal neurons in vitro and in vivo from 3-nitropropionic acid toxicity. J Comp Neurol 425: 471–478.

Liot G, Bossy B, Lubitz S, Kushnareva Y, Sejbuk N, Bossy-Wetzel E (2009). Complex II inhibition by 3-NP causes mitochondrial fragmentation and neuronal cell death via an NMDA- and ROS-dependent pathway. Cell Death Differ 16: 899–909.

Menzies FM, Cookson MR, Taylor RW, Turnbull DM, Chrzanowska-Lightowlers ZM, Dong L *et al.* (2002). Mitochondrial dysfunction in a cell culture model of familial amyotrophic lateral sclerosis. Brain 125: 1522–1533.

Mozdy AD, McCaffery JM, Shaw JM (2000). Dnm1p GTPase-mediated mitochondrial fission is a multi-step process requiring the novel integral membrane component Fis1p. J Cell Biol 151: 367–380.

Nishimura M, Okimura Y, Fujita H, Yano H, Lee J, Suzaki E *et al.* (2008). Mechanism of 3-nitropropionic acid-induced membrane permeability transition of isolated mitochondria and its suppression by L-carnitine. Cell Biochem Funct 26: 881–891.

Otsuga D, Keegan BR, Brisch E, Thatcher JW, Hermann GJ, Bleazard W *et al.* (1998). The dynamin-related GTPase, Dnm1p, controls mitochondrial morphology in yeast. J Cell Biol 143: 333–349.

Panov AV, Gutekunst CA, Leavitt BR, Hayden MR, Burke JR, Strittmatter WJ *et al.* (2002). Early mitochondrial calcium defects in Huntington's disease are a direct effect of polyglutamines. Nat Neurosci 5: 731–736.

Perez-Alvarez S, Solesio ME, Manzanares J, Jordan J, Galindo MF (2009). Lactacystin requires reactive oxygen species and Bax redistribution to induce mitochondria-mediated cell death. Br J Pharmacol 158: 1121–1130.

Perez-Alvarez S, Cuenca-Lopez MD, de Mera RM, Puerta E, Karachitos A, Bednarczyk P *et al.* (2010). Methadone induces necrotic-like cell death in SH-SY5Y cells by an impairment of mitochondrial ATP synthesis. Biochim Biophys Acta 1802: 1036–1047.

Petronilli V, Miotto G, Canton M, Brini M, Colonna R, Bernardi P *et al.* (1999). Transient and long-lasting openings of the mitochondrial permeability transition pore can be monitored directly in intact cells by changes in mitochondrial calcein fluorescence. Biophys J 76: 725–734.

Puyal J, Ginet V, Grishchuk Y, Truttmann AC, Clarke PG (2011). Neuronal autophagy as a mediator of life and death: contrasting roles in chronic neurodegenerative and acute neural disorders. Neuroscientist 18: 224–236.

Skulachev VP, Bakeeva LE, Chernyak BV, Domnina LV, Minin AA, Pletjushkina OY *et al.* (2004). Thread-grain transition of mitochondrial reticulum as a step of mitoptosis and apoptosis. Mol Cell Biochem 256-257: 341–358.

Smaili SS, Hsu YT, Sanders KM, Russell JT, Youle RJ (2001). Bax translocation to mitochondria subsequent to a rapid loss of mitochondrial membrane potential. Cell Death Differ 8: 909–920.

Tanaka A, Youle RJ (2008). A chemical inhibitor of DRP1 uncouples mitochondrial fission and apoptosis. Mol Cell 29: 409–410.

Xue L, Fletcher GC, Tolkovsky AM (1999). Autophagy is activated by apoptotic signalling in sympathetic neurons: an alternative mechanism of death execution. Mol Cell Neurosci 14: 180–198.

Yu L, Wan F, Dutta S, Welsh S, Liu Z, Freundt E *et al.* (2006). Autophagic programmed cell death by selective catalase degradation. Proc Natl Acad Sci USA 103: 4952–4957.

Zhang XD, Wang Y, Zhang X, Han R, Wu JC, Liang ZQ *et al.* (2009). p53 mediates mitochondria dysfunction-triggered autophagy activation and cell death in rat striatum. Autophagy 5: 339–350.